Journal of Newviews in Engineering and Technology (JNET)
Vol 2, Issue 1, March, 2020
Available online at http://www.rsujnet.org/index.php/publications/2020-edition

Modeling of Eccentricity and Performance of Three-Phase Induction Motors

Olalowo S. Olaleye[1], Christopher O. Ahiakwo[2], Dikio C. Idoniboyeobu[3], and Sunny Orike[4]
Department of Electrical Engineering, Rivers State University, Port Harcourt
[1]olaleye.samuel@ust.edu.ng, [2]ahiakwo.christopher@ust.edu.ng,
[3]idoniboyeobu.d@ust.edu.ng, [4]orike.sunny@ust.edu.ng

ABSTRACT:

This paper modelled the eccentricity in three-phase induction motors and the accompanying performance. The geometry of three-phase asynchronous induction motor was utilized to calculate dynamic electromagnetic torque and inductances for the purpose of performance improvement. The position-dependent variation of the mechanical energy was applied to the rotor through the air gap which generates the mutual inductance across the stator-rotor circuitry. The entire six-by-six inductance matrix modelled for the non-concentric three-phase induction motor was analytically differentiated and used to model the torque equation for the eccentric motor. The approach was simulated in MATLAB and ratified with an eccentricity degree of zero (non-existent) which tallied and rhymed with that gotten for a healthy induction motor. Results obtained show that an eccentric motor rotor does not accelerate uniformly, but glitches and flickers intermittently until it attains a maximum speed of about 320 rad/sec, whereas for the healthy motor, the rotor accelerates uniformly from rest to peak giving rise to a load-less motor speed of 0.33sec. For eccentricity degrees greater than 0.7, the air gap function for a non-concentric three-phase induction motor goes higher than 1.0 at some points and hits zero at lowest values thereby validating that the displacement of the rotor position from the normal is directly proportional to the degree of eccentricity.

KEYWORDS: Air gaps, Electrical machines, Inductance, Induction motors, Windings.

Cite This Article: Olaleye, O. S., Ahiakwo, C. O., Idoniboyeobu, D. C., and Orike, S. (2020). Modeling of Eccentricity and Performance of Three-Phase Induction Motors. *Journal of Newviews in Engineering and Technology (JNET)*, 2 (1), 97-108.

1. INTRODUCTION:

In industrial applications, 35% - 40% of generated electrical energy is consumed by electrical motors, (Nandi *et al.*, 2005). Electrical machines are electromechanical energy converting equipment using electromagnetic forces. They are broadly classified as motors and generators, (Aderiano, 2006). An electrical motor can either be a synchronous motor or asynchronous (induction) motors.

The popularity of induction motors is due to their robustness, high efficiency, and low cost (Bouchikhi *et al.*, 2013). Induction motors are very reliable as they require minimal maintenance and have high efficiency (Ferreira & Almeida, 2006). Additionally, the wide range of motor power ranging from hundreds of watts to megawatt adequately satisfy most industrial production processes (Almeida *et al.*, 2014). Besides, due to non-uniformity of the air gap between stator-inner surface and rotor-outer surface motor, eccentricity faults also occur. Many researches on electrical machines summarily show, that 80% of mechanical faults lead to the rotor eccentricity, (Sen, 1999). Any eccentricity in the machine will create excessive mechanical stress and cause more fatigue in the bearings (Stephan, 2005).

Basically, there are there types of eccentricities and a hybrid in induction motors, viz:

i. Static Eccentricity: A rotor eccentricity where the rotor rotates on its own axis but not at the centre of the stator bore which causes the 2-times supply frequency force faults also occur. to act towards the direction of the narrowest air gap (Dorrell, 1993; Joksimovic, 2017). This is shown in Fig. 1(a).
ii. Dynamic Eccentricity: Here, the rotor rotates at the centre of the stator bore axis and not on its own axis, in which case the minimum air gap rotates with the rotor rotating frequency (Silwal *et al,* 2016). This is depicted in Fig. 1(b)

Journal of Newviews in Engineering and Technology (JNET)
Vol 2, Issue 1, March, 2020
Available online at http://www.rsujnet.org/index.php/publications/2020-edition

(a) (b)

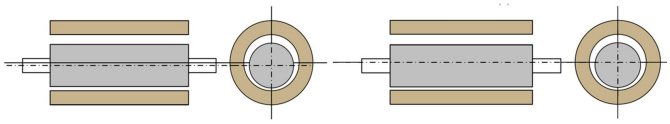

Fig 1 Two Basic Types of Eccentricity: (a) Static (b) Dynamic (Chuan & Shek, 2016).

iii. Mixed Eccentricity: This precisely is the detectable and locatable eccentricity in real life because in a faulty induction motor both the static and dynamic eccentricities could be observed and discovered (Arkkio *et al*., 2016). Really, it simply means the hybrid/combination of both static and dynamic eccentricities (Polat *et al.,* 2017). Effectively, in this integrated situation of eccentricity, the air gap status changes in two ways: one in its severity and the spatial spread of the non-uniformity.

The degree of eccentricity, ε, is the ratio between the mean air gap length, g0 and the length of the eccentricity rotor misalignment, e. The degree of eccentricity can be written as:

$$\varepsilon = \frac{e}{g_0} \qquad (1)$$

2. MATERIALS AND METHODS:

The development of phase variable model of induction motors will naturally lead to an analytical model that can be used for design and performance prediction under all conditions. Although the d-q model is popular and has found enough applications in control and performance analysis, it has limited applications when faults, uncommon performances and performance under eccentricity is concerned. The popularity of the d-q model stems from the ease of performance prediction in absence of dependence of inductances on rotor position and the natural way the model lends itself readily for steady-state analysis. For clarity, even though it is well known that self-inductances of stator and rotor windings of polyphase induction machines are independent of rotor position, the torque producing components, i.e. the stator-mutual inductances are clearly dependent on rotor positions. It is this dependence that the d-q transformation tends to eliminate. Eliminating this dependence allows the model an ease of interpretation and solution as several numerical methods like Runge-Kutta, Heuns and several other ones can come into play. But stripping the machine model of this dependence relies on an assumption that the air gap is always uniform throughout the machine operation. This uniformity does not obtain in practice since every electric machine operates under some level of eccentricity.

Eccentricity means the departure of the air gap from this assumed uniformity. To establish a benchmark, we first formulated the model of the machine with a uniform air gap and then modified this for eccentric conditions. For this reason, we modeled three-phase induction motors in the KW range as such machines usually have high inertia rotor which are often susceptible to eccentricity.

2.1 The Model of Uniform Air gap Polyphase Induction Motor:

Fig. 2 shows the winding distribution for one pole-pitch of the machine considered in this model while Fig. 3 shows the conceptual electrical diagram. Now, consider a three-phase induction motor with distributed three phase windings on the stator and another three phase windings on the rotor as shown in Fig. 2. In Fig. 3, the stator windings are connected to the power supply. It is obvious that the rotor windings must be short-circuited if the machine will start directly from line. In both the stator and the rotor, the windings are co-phasally distributed, i.e. each winding is displaced from one another by 120 degrees.

Obe (2010) established for any phase of the three-phase windings of (2):

$$N_x = \sum_{n=1,3,5,\ldots}^{n} \frac{4 N_T \, k_{wn}}{N_x} cosp_r \, n \left(\varphi - k \, \frac{2\pi}{p_r \, m}\right) \qquad (2)$$

Where:

k_{dn} = distribution factor k_{pn} = pitch factors q = the number of slots per pole per phase τ_p = the pole pitch and W = the coil width. For simplicity, we considered only the fundamental component of the

Journal of Newviews in Engineering and Technology (JNET)
Vol 2, Issue 1, March, 2020
Available online at http://www.rsujnet.org/index.php/publications/2020-edition

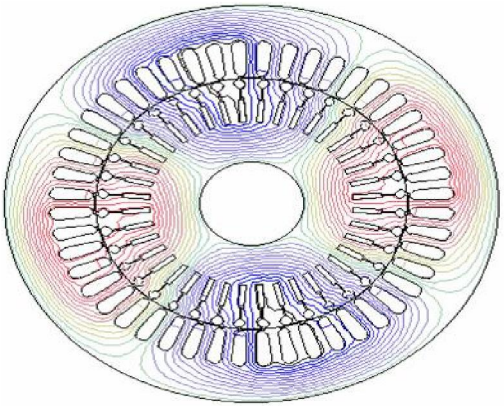

Fig 2 One Pole-Pitch Winding Distribution of an Induction Motor (Wasynczuk *et al.*, 2013)

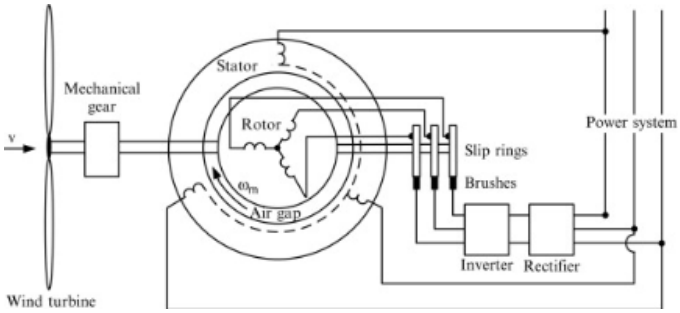

Fig 3 Conceptual Electrical Circuitry of an Induction Motor (Dorrell *et al.*, 2013)

$$k_{wn} = k_{dn} \cdot k_{wn} = \frac{\sin\left(\frac{n\pi}{2m}\right)}{q \sin\left(\frac{n\pi}{2qm}\right)} \sin\left(n \frac{W\pi}{\tau_r 2}\right) \quad (3)$$

windings and then assumed that each of the windings is fully pitched (k_{w1}=1). Based on these, the MMF per ampere or winding functions of the stator and rotor windings are:

$$N_{AS} = N_S cos(p_r \varphi) \quad (4)$$

$$N_{BS} = N_S cos\left(p_r \varphi - \frac{2\pi}{3}\right) \quad (5)$$

$$N_{CS} = N_S cos\left(p_r \varphi - \frac{4\pi}{3}\right) \quad (6)$$

It is obvious from equations (4) to (6) that N_s is the amplitude of the fundamental component of the magnetomotive force (MMF) waveform for the stator windings, the subscripts A, B, and C relate directly to the phases A, B and C.

$$N_{AR} = N_r \cos[\, p_r\, (\varphi - \theta_r)] \quad (7)$$

$$N_{BR} = N_r \cos[\, p_r\, (\varphi - \theta_r) - \frac{2\pi}{3}\,] \quad (8)$$

$$N_{CR} = N_r \cos[\, p_r\, (\varphi - \theta_r) - \frac{4\pi}{3}\,] \quad (9)$$

Here, θ_r is the rotor circumferential position, known as rotor position. The air gap function of a normal induction motor is given by:

$$g(\varphi, \theta_r) = g_0 \quad (10)$$

Modeling of Inductances for Healthy 3-Phase Induction Motors

Since the machine has three windings on the stator, designated as AS, BS and CS and another three on the rotor designated as AR, BR and CR, there is thus:

i. a 3 x 3 matrix of stator inductances denoted as L_{SS},
ii. a 3 x 3 matrix of rotor inductances, denoted as L_{RR}
iii. a 3 x 3 matrix of stator-rotor inductances, denoted as L_{SR} and
iv. a 3 x 3 matrix of rotor-stator inductances, denoted as L_{RS}

The inductance expressions individually derived and then put together to form the four matrices identified above. Notably, (c) and (d) above are the same and therefore we have three inductance matrices to determine. Any inductance of this machine can be deduced by using the winding function theory which can be simplified as:

$$L_{XY}(\theta_r) = \mu_0 RL \int_0^{2\pi} \frac{N_X(\varphi) \times N_Y(\varphi)}{g(\varphi, \theta_r)} d\varphi \quad (11)$$

Where μ_o is the permeability of free space, R is the effective radius of the air gap, L is the machine stack length, N_X and N_Y are the winding functions for windings X and Y respectively which depend solely on the spatial stator circumferential position φ and g is the air gap function which should depend on φ and position of rotor θ_r.

Stator Inductances

The self-inductance of stator phase A winding can be readily determined from (10) as:

Journal of Newviews in Engineering and Technology (JNET)
Vol 2, Issue 1, March, 2020
Available online at http://www.rsujnet.org/index.php/publications/2020-edition

$$L_{ASAS} = \mu_0 RL \int_0^{2\pi} \frac{N_{AS}(\varphi) \times N_{AS}(\varphi)}{g(\varphi, \theta_r)} d\varphi \quad (12)$$

$$= \mu_0 RL \int_0^{2\pi} \frac{N_S cos(p_r\varphi) \times N_S cos(p_r\varphi)}{g} d\varphi \quad (13)$$

$$= \frac{\mu_0 RL\pi N_S^2}{g_0} \quad (14)$$

Using similar approach, we can write that:

$$L_{BSBS} = L_{CSCS} = \frac{\mu_0 RL\pi N_S^2}{g} \quad (15)$$

$$L_{ASBS} = L_{BSAS} = L_{BSCS} = L_{CSBS} = L_{ASCS} = L_{CSAS} \quad (16)$$

$$= -\frac{\mu_0 RL\pi N_S^2}{2g_0} \quad (17)$$

Combining these inductances, stator inductance L_{SS} evolves as:

$$L_{SS} = \begin{bmatrix} L_{ASAS} & L_{ASBS} & L_{ASCS} \\ L_{BSAS} & L_{BSBS} & L_{BSCS} \\ L_{CSAS} & L_{CSBS} & L_{CSCS} \end{bmatrix} \quad (18)$$

$$= L_{ms} \begin{bmatrix} 1 & -\frac{1}{2} & -\frac{1}{2} \\ -\frac{1}{2} & 1 & -\frac{1}{2} \\ -\frac{1}{2} & -\frac{1}{2} & 1 \end{bmatrix} \quad (19)$$

Where: $L_{ms} = \frac{\mu_0 RL\pi N_S^2}{g_0}$ (20)

Rotor Inductances

Adopting (11) and a suitable combination of (7) to (10), we can also obtain the rotor inductance matrix via the same procedure and have L_{RR} as:

$$L_{RR} = \begin{bmatrix} L_{ARAR} & L_{ARBR} & L_{ARCR} \\ L_{BRAR} & L_{BRBR} & L_{BRCR} \\ L_{CRAR} & L_{CRBR} & L_{CRCR} \end{bmatrix} \quad (21)$$

$$\begin{bmatrix} 1 & -\frac{1}{2} & -\frac{1}{2} \\ -\frac{1}{2} & 1 & -\frac{1}{2} \\ -\frac{1}{2} & -\frac{1}{2} & 1 \end{bmatrix} \quad (22)$$

Where: $L_{mr} = \frac{\mu_0 RL\pi N_R^2}{g_0}$ (23)

Rotor-to-Stator Inductances

Next set of inductance expressions to be derived are the rotor-to-stator inductances (same as stator to rotor inductances). It is this set of inductances that link all components of the matrix mutual inductances. These are obtained by combining the stator and rotor MMFs with the air gap via (11). We can find each one individually, again by integration:

$$L_{ASAR}(\theta_r) = \mu_0 RL \int_0^{2\pi} \frac{N_{AS}(\varphi) \times N_{AR}(\varphi)}{g(\varphi, \theta_r)} d\varphi \quad (24)$$

$$= \mu_0 RL \int_0^{2\pi} \frac{N_S cos(p_r\varphi) \times N_R cos(p_r(\varphi - \theta_r))}{g_0} d\varphi \quad (25)$$

$$= \frac{\mu_0 RL\pi N_S N_r}{g_0} \cos(\theta_r) \quad (26)$$

Similarly, L_{ASBR} will be:

$$L_{ASBR}(\theta_r) = \mu_0 RL \int_0^{2\pi} \frac{N_{AS}(\varphi) \times N_{BR}(\varphi)}{g(\varphi, \theta_r)} d\varphi \quad (27)$$

$$= \mu_0 RL \int_0^{2\pi} \frac{N_S cos(p_r\varphi) \times N_R cos\left(p_r(\varphi - \theta_r) - \frac{2\pi}{3}\right)}{g_0} d\varphi \quad (28)$$

$$= \frac{\mu_0 RL\pi N_S N_r}{g_0} \cos\left(\theta_r + \frac{2\pi}{3}\right) \quad (29)$$

$$= L_{sr} \begin{bmatrix} \cos(\theta_r) & \cos\left(\theta_r + \frac{2\pi}{3}\right) & \cos\left(\theta_r - \frac{2\pi}{3}\right) \\ \cos\left(\theta_r - \frac{2\pi}{3}\right) & \cos(\theta_r) & \cos\left(\theta_r + \frac{2\pi}{3}\right) \\ \cos\left(\theta_r + \frac{2\pi}{3}\right) & \cos\left(\theta_r - \frac{2\pi}{3}\right) & \cos(\theta_r) \end{bmatrix} \quad (31)$$

Where: $L_{sr} = \frac{\mu_0 RL\pi N_S N_r}{g_0}$ (32)

The stator and rotor inductances are not function of rotor position, but the stator-to-rotor inductances are.

Voltage Equations

Since we have analytically conceived that the three-phase induction motor has three-phase distributed windings and displaced from one another by 120 degrees, each of the stator and rotor winding circuits have the same form of voltage equations. These equations are written according to KVL in the form:

$$V = IR + \frac{d}{dt}(LI) \quad (33)$$

Here, V is the voltage vector which can be written as:

$$V = [V_S \ V_R] = [V_{AS} \ V_{BS} \ V_{CS} \ V_{AR} \ V_{BR} \ V_{CR}]^T \quad (34)$$

I, the current vector also given as:

$$I = [I_S \ I_R] = [I_{AS} \ I_{BS} \ I_{CS} \ I_{AR} \ I_{BR} \ I_{CR}]^T \quad (35)$$

The resistance matrix is a six by six matrix of which each winding resistance occupies a whole row and column. It has the form:

Journal of Newviews in Engineering and Technology (JNET)
Vol 2, Issue 1, March, 2020
Available online at http://www.rsujnet.org/index.php/publications/2020-edition

$$R = \begin{bmatrix} R_{AS} & 0 & 0 & & & \\ 0 & R_{BS} & 0 & & zero(3x3) & \\ 0 & 0 & R_{CS} & & & \\ & & & R_{AR} & 0 & 0 \\ & zero(3x3) & & 0 & R_{BR} & 0 \\ & & & 0 & 0 & R_{CR} \end{bmatrix} \quad (36)$$

$$R = diag[R_s\ R_s\ R_s\ R_r\ R_r\ R_r] \quad (37)$$

The inductance L given in (33) is expressed as:

$$L = \begin{bmatrix} L_{SS} & L_{SR} \\ L_{RS} & L_{RR} \end{bmatrix} \quad (38)$$

Where, L_{SS}, L_{SR}, L_{RS} and L_{RR} are as given in (19), (22) and (31).

Solution of the Voltage Equation

The voltage equation (33) of the three-phase induction motor under study is a differential equation. Owing to this, the most amenable way of solving it is by integration with solution will be aimed at determining the current I. With the inductance L being a function of rotor position (on account of the stator-rotor mutual inductance), one can re-write (33) as:

$$\boldsymbol{V = IR + L(\theta_r)\frac{dI}{dt} + I\frac{d}{dt}\left(L(\theta_r)\right)} \quad (39)$$

But,

$$\frac{d}{dt} = \frac{d}{d\theta_r} \times \frac{d\theta_r}{dt} \quad (40)$$

Also,

$$\frac{d\theta_r}{dt} = \omega \quad (41)$$

Equation (39) becomes:

$$\boldsymbol{V = IR + L(\theta_r)\frac{dI}{dt} + I\omega\frac{d}{d\theta_r}\left(L(\theta_r)\right)} \quad (42)$$

Making $\frac{dI}{dt}$ subject of formula in (42):

$$\frac{dI}{dt} = \frac{V - I\left(R - \omega\frac{dL(\theta_r)}{d\theta_r}\right)}{L(\theta_r)} \quad (43)$$

$$= \left[V - I\left(R - \omega\frac{dL(\theta_r)}{d\theta_r}\right)\right]\left(L(\theta_r)\right)^{-1} \quad (44)$$

Equation (42) shows that to calculate $\frac{dI}{dt}$ at every time step, the derivative of the 6 x 6 inductance matrix and its inverse needs to be calculated prior to determining the algebra of (44).This is very cumbersome in view of the usual minuteness of time variation for which such calculations have to be performed in order to yield a very accurate solution. However, this is the price to be paid for discarding the popular dimensionless d-q model in favour of this dimension-based phase variable model.

The Torque Equation in Phase Variables for the Healthy Induction Motor

Deducing from co-energy, the torque equation of the induction machine under consideration can be found from:

$$T_e = \frac{1}{2}[I]^T\frac{\partial L(\theta_r)}{\partial\theta_r}[I] \quad (45)$$

We now know that for this machine, only L_{SR} = L_{SR} component of L have dependence on θ_r, as only this component of inductance will produce torque. Hence, (45) can be reduced to:

$$\boldsymbol{T_e = \frac{1}{2}[I_S]^T\frac{\partial L_{SR}(\theta_r)}{\partial\theta_r}[I_R]} \quad (46)$$

$$[I_S]^T = [I_{AS}\ .\ I_{BS}\ .I_{CS}]^T \quad (47)$$

$$[I_R]^T = [I_{AR}\ .\ I_{BR}\ .I_{CR}]^T \quad (48)$$

And, L_{SR} (θ_r) is the inductance matrix in phase variable form given in (31). The mechanical equation of motion of the moving rotor is needed too and is:

$$p\omega_r = p_r \times \frac{T_e - T_L}{2J} \quad (49)$$

In (49), T_L is the load torque and J is the moment of inertia of the moving rotor and any accompanying load. The derivative of the stator to mutual inductance matrix is needed as in (44) and in evaluation of the dynamic torque in (46). This derivative has been evaluated as:

$$\frac{dL_{SR}}{d\theta_r} = \frac{dL_{RS}}{d\theta_r} \quad (50)$$

Journal of Newviews in Engineering and Technology (JNET)
Vol 2, Issue 1, March, 2020
Available online at http://www.rsujnet.org/index.php/publications/2020-edition

$$= \begin{bmatrix} L_{ASAR} & L_{ASBR} & L_{ASCR} \\ L_{BSAR} & L_{BSBR} & L_{BSCR} \\ L_{CSAR} & L_{CSBR} & L_{CSCR} \end{bmatrix} \quad (51)$$

$$= -L_{sr} \begin{bmatrix} \sin(\theta_r) & \sin\left(\theta_r + \frac{2\pi}{3}\right) & \sin\left(\theta_r - \frac{2\pi}{3}\right) \\ \sin\left(\theta_r - \frac{2\pi}{3}\right) & \sin(\theta_r) & \sin\left(\theta_r + \frac{2\pi}{3}\right) \\ \sin\left(\theta_r + \frac{2\pi}{3}\right) & \sin\left(\theta_r - \frac{2\pi}{3}\right) & \sin(\theta_r) \end{bmatrix} \quad (52)$$

In simulating the 3-phase induction motor eccentric model, a set of parameters of a three-phase induction motor was used. For this study, we chose a three- phase induction motor whose parameters are shown in Table 1. The simulation results showing rotor speed, stator currents, rotor currents, electromagnetic torque and dynamic speed-torque plots are shown in Figs. 5, 7, 9, 11 & 13.

2.2 Model of the Eccentric Induction Motor

Consider Fig. 4 which shows the schematic cross-sectional diagram of both a healthy and eccentric induction motor. The departure from uniform air gap in the eccentric motor can be caused by any of the following: misalignment during installation or wear due to long period of operation of the bearing, unbalanced magnetic pull owing to minor inaccuracies in slotting positions around the stator periphery, misalignment of the load or rotor axis or mechanical resonance in some critical loads especially for machines that run under varying load conditions, etc.

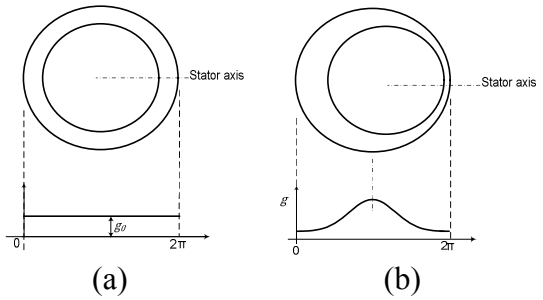

(a) (b)

Fig 4 Schematic diagram of induction motor showing the air gap functions under (a) healthy and (b) eccentric modes

Under eccentric conditions, the volume of the air gap will remain the same, but the air gap becomes smaller in some regions and then becomes bigger in other regions. This will naturally mean that the energy conversion will not change but the torque, fluxes, currents and other state variables will assume irregular shapes which will then lead to a distorted operation of the motor. The degree of these distortions will depend on the magnitude of eccentricity. Within the limits of manufacturing error, one can rightfully say that no induction motor can operate in a healthy condition and therefore every motor operates under eccentricity. It is the degree of eccentricity that therefore matters.

It is easy to see that the air gap of the normal (or healthy machine) shown in Fig. 4(a) is independent of the position of the rotor – the air gap is uniform and can be easily described as (10). In the case of the eccentric motor, the air gap is as shown in Fig. 4(b). Using curve-fitting techniques, it is shown that the model of the air gap becomes:

(53)

Here, g0 is the air gap under normal conditions, ρ is the degree of eccentricity which ranges from 0.0 (healthy conditions) to 1.0 (highest level of eccentricity in which the rotor statically rubs on the stator. Equation (53) is derived on the condition that the deviation in the rotor does not affect the actual shape of the rotor; rather, it only affects its displacement from original mechanical rotating axis by virtue of any of the causes of eccentricity mentioned earlier. From literature, eccentricity degrees of 0.7 and above are not tolerable because centrifugal forces will further tend to move the rotor further to rub on the stator if eccentricities reach such high values (Joksimovic *et al.*, 2000; Faiz & Ojaghi, 2009; Faiz *et al.*, 2010).

To validate and visualize the extent of rotor departure from normalcy as given in equation (53), an m-file was developed in MATLAB for eccentricity values ranging from 0.0 to 1.0 in steps of 0.2 and for g 0 = 0.7mm. The graphs generated for this air gap condition are as shown in Fig. 6.

Stator Inductances

Using the already deduced winding MMFs and (3), the stator inductances were:

$$EL_{ASAS}(\theta_r) = \mu_0 RL \int_0^{2\pi} \frac{N_{AS}(\varphi) \times N_{AS}(\varphi)}{g(\varphi,\theta_r)} d\varphi \quad (54)$$

$$= \mu_0 RL \int_0^{2\pi} \frac{N_s cos(p_r\varphi) \times N_s cos(p_r\varphi)}{g_0(1-\rho\cos(\theta_r))} d\varphi \quad (55)$$

$$= \frac{\mu_0 RL\pi N_s^2}{g_0(1-\rho\cos(\theta_r))} \quad (56)$$

Using similar approach, we can write that:

$$EL_{ASBS} = -\frac{\mu_0 RL\pi N_s^2}{2g_0(1-\rho\cos(\theta_r))} \quad (57)$$

$$EL_{SS} = \begin{bmatrix} EL_{ASAS} & EL_{ASBS} & EL_{ASCS} \\ EL_{BSAS} & EL_{BSBS} & EL_{BSCS} \\ EL_{CSAS} & EL_{CSBS} & EL_{CSCS} \end{bmatrix} \quad (58)$$

$$= EL_{ms} \begin{bmatrix} 1 & -\frac{1}{2} & -\frac{1}{2} \\ -\frac{1}{2} & 1 & -\frac{1}{2} \\ -\frac{1}{2} & -\frac{1}{2} & 1 \end{bmatrix} \quad (59)$$

Where: EL_{ms} in this case is,

$$EL_{ms} = \frac{\mu_0 RL\pi N_s^2}{g_0(1-\rho\cos(\theta_r))} \quad (60)$$

Rotor Inductances

The rotor inductances were also derived to be in the form:

$$EL_{RR} = \begin{bmatrix} EL_{ARAR} & EL_{ARBR} & EL_{ARCR} \\ EL_{BRAR} & EL_{BRBR} & EL_{BRCR} \\ EL_{CRAR} & EL_{CRBR} & EL_{CRCR} \end{bmatrix} \quad (61)$$

$$= EL_{mr} \begin{bmatrix} 1 & -\frac{1}{2} & -\frac{1}{2} \\ -\frac{1}{2} & 1 & -\frac{1}{2} \\ -\frac{1}{2} & -\frac{1}{2} & 1 \end{bmatrix} \quad (62)$$

Where, EL_{mr} in this case is:

$$EL_{mr} = \frac{\mu_0 RL\pi N_R^2}{g_0(1-\rho\cos(\theta_r))} \quad (63)$$

Stator to Rotor Inductances

The stator-to-rotor inductances require a careful handling on the grounds that the rotor-position dependent air gap is now to be integrated with the MMF equations which are also dependent on rotor position. The inductances are found as follows:

$$= \mu_0 RL \int_0^{2\pi} \frac{N_s cos(p_r\varphi) \times N_R cos(p_r(\varphi-\theta_r))}{g_0(1-\rho\cos(\theta_r))} d\varphi \quad (65)$$

$$= \frac{\mu_0 RL\pi N_s N_r}{g_0(1-\rho\cos(\theta_r))} \cos(\theta_r) \quad (66)$$

Similarly, EL_{ASBR} will be:

$$EL_{ASBR}(\theta_r) = \mu_0 RL \int_0^{2\pi} \frac{N_{AS}(\varphi) \times N_{BR}(\varphi,\theta_r)}{g(\varphi,\theta_r)} d\varphi \quad (67)$$

$$= \mu_0 RL \int_0^{2\pi} \frac{N_s cos(p_r\varphi) \times N_R cos\left(p_r(\varphi-\theta_r)-\frac{2\pi}{3}\right)}{g_0(1-\rho\cos(\theta_r))} d\varphi \quad (68)$$

$$= \frac{\mu_0 RL\pi N_s N_r}{g_0(1-\rho\cos(\theta_r))} \cos\left(\theta_r + \frac{2\pi}{3}\right) \quad (69)$$

Progressively, the stator to rotor inductance matrix:

$$EL_{SR} = EL_{RS} \quad (70)$$

$$= \begin{bmatrix} EL_{ASAR} & EL_{ASBR} & EL_{ASCR} \\ EL_{BSAR} & EL_{BSBR} & EL_{BSCR} \\ EL_{CSAR} & EL_{CSBR} & EL_{CSCR} \end{bmatrix} \quad (71)$$

$$= EL_{sr} \begin{bmatrix} \cos(\theta_r) & \cos\left(\theta_r + \frac{2\pi}{3}\right) & \cos\left(\theta_r - \frac{2\pi}{3}\right) \\ \cos\left(\theta_r - \frac{2\pi}{3}\right) & \cos(\theta_r) & \cos\left(\theta_r + \frac{2\pi}{3}\right) \\ \cos\left(\theta_r + \frac{2\pi}{3}\right) & \cos\left(\theta_r - \frac{2\pi}{3}\right) & \cos(\theta_r) \end{bmatrix} \quad (72)$$

Where:

$$EL_{sr} = \frac{\mu_0 RL\pi N_s N_r}{g(1-\rho\cos(\theta_r))} \quad (73)$$

It is now necessary to plot the inductances with respect to rotor position for the eccentric machine. Thus, Figs. 14 to 18 show the inductances for eccentricities of ρ = 0.1 and 0.4.

Derivative of Machine Inductance Matrices for the Eccentric Motor

For the normal induction motor, only the derivative of L_{SR} is needed as derivatives of L_{SS} and L_{RR} will become zero on the account of their non-dependence on Θ_r. However, for the eccentric motor, all the inductance matrices EL_{SS}, EL_{RR} and EL_{SR} will need to be differentiated as they will be needed while evaluating (44) in the

Journal of Newviews in Engineering and Technology (JNET)
Vol 2, Issue 1, March, 2020
Available online at http://www.rsujnet.org/index.php/publications/2020-edition

time-stepping simulation.
These derivatives are:

$$\frac{dEL_{SS}}{d\theta_r} = -\frac{\mu_0 RL\pi N_s^2 \rho sin(\theta_r)}{g(\rho cos(\theta_r)-1)^2} \times \begin{bmatrix} 1 & -\frac{1}{2} & -\frac{1}{2} \\ -\frac{1}{2} & 1 & -\frac{1}{2} \\ -\frac{1}{2} & -\frac{1}{2} & 1 \end{bmatrix} \quad (74)$$

$$\frac{dEL_{RR}}{d\theta_r} = -\frac{\mu_0 RL\pi N_r^2 \rho sin(\theta_r)}{g(\rho cos(\theta_r)-1)^2} \times \begin{bmatrix} 1 & -\frac{1}{2} & -\frac{1}{2} \\ -\frac{1}{2} & 1 & -\frac{1}{2} \\ -\frac{1}{2} & -\frac{1}{2} & 1 \end{bmatrix} \quad (75)$$

$$\frac{dEL_{SR}}{d\theta_r} = \frac{dEL_{RS}}{d\theta_r} \quad (76)$$

$$= \frac{\mu_0 RL\pi N_s N_r}{g(\rho cos(\theta_r)-1)^2} \begin{bmatrix} -\sin(\theta_r) & f_p(\rho,\theta_r) & f_n(\rho,\theta_r) \\ f_n(\rho,\theta_r) & -\sin(\theta_r) & f_p(\rho,\theta_r) \\ f_p(\rho,\theta_r) & f_n(\rho,\theta_r) & -\sin(\theta_r) \end{bmatrix} \quad (77)$$

Where:

$$f_p(\rho,\theta_r) = \left(\frac{\sqrt{3}}{2}\rho - sin\left(\theta_r + \frac{2\pi}{3}\right)\right) \quad (78)$$

And,

$$f_n(\rho,\theta_r) = \left(sin\left(\frac{2\pi}{3} - \theta_r\right) - \frac{\sqrt{3}}{2}\rho\right) \quad (79)$$

Torque Equation of the Eccentric IM

Equation (46) deduced from co-energy considerations is still valid for torque of the eccentric motor provided that the air gap function is clearly embedded in the inductance calculations prior to taking the derivatives of the torque expression. It should be emphasized here that the entire machine inductance matrix which is of size 6 by 6 is now used in the torque calculation as against the use of L_{SR} only in normal induction motor. Using (74), (75) and (76), the torque equation evaluated as in (46) will lead to an expression that is too long to write here. Suffice it to say that in the phase variable model under consideration, this expression is not needed as it cannot ordinarily on its own lead to any physical interpretation of the machine performance.

3. RESULTS AND DISCUSSION:

For this study, we chose an 11KW three-phase induction motor whose parameters are shown in Table 1. The simulation results showing rotor speed, stator currents, rotor currents, electromagnetic torque and dynamic speed-torque plots are shown in Figs. 6, 8, 10, 12 and 14.

3.1 Simulation of the Eccentric 3-Phase Induction Motor

We undertook the simulation using the same set of parameters defined in Table 1 but for differing degrees of eccentricity. As a base check, a value of ρ = 0 is chosen and the results obtained tallies with that of a healthy induction motor studied above. The simulation results for Eccentric 3-Phase Induction motor showing rotor speed, stator currents, rotor currents, electromagnetic torque and dynamic speed-torque plots are depicted in Figs. 6, 8, 10, 12 and 14 depict how the eccentricity fault impact on the respective parameters studied.

Table 1: Parameters of the Simulated 11KW 3-Phase Wound Rotor Induction Motor

Parameter	Value and Unit
No of poles, p	6
Motor resistance, R	115mm
Air gap length, L	240mm
Rotor turns, Nr	100 turns
Stator turns, Ns	135 turns
Frequency rated, f	50Hz
Stator resistance, Rs	0.85Ω
Rotor bar resistance, Rr	0.23Ω
Rotor inertia, J	1.56kg/m^3
Stator inductance, Lls	0.0024mH
Rotor inductance, Llr	0.0024mH

Figs. 5, 7, 9 and 11 are for the healthy 3-phase motor performance. To validate and visualize the extent of rotor departure from normalcy, an m-file was developed in MATLAB for eccentricity values ranging from 0.0 to 1.0 in steps of 0.2 and for g_0= 0.7 mm. The graphs generated for this air gap condition are as shown in Fig 5.

Journal of Newviews in Engineering and Technology (JNET)
Vol 2, Issue 1, March, 2020
Available online at http://www.rsujnet.org/index.php/publications/2020-edition

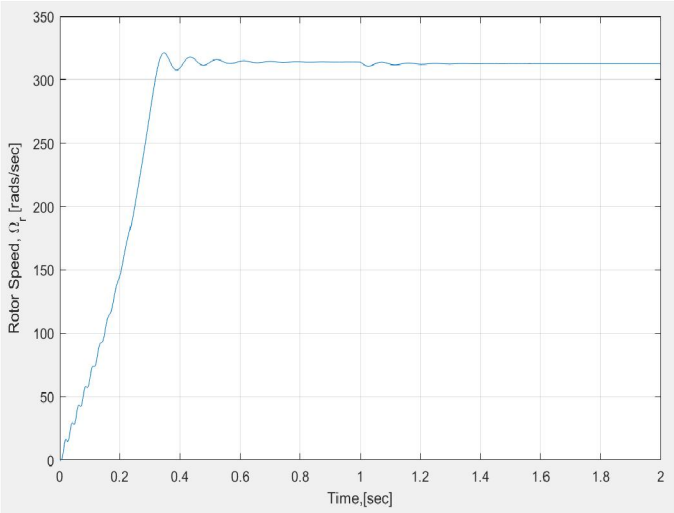

Fig 5 Rotor Speed Waveform from Simulated Healthy 3-Phase Induction Motor

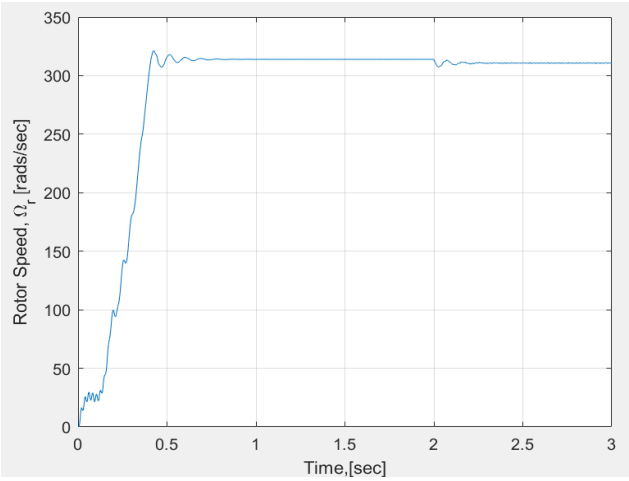

Fig 6 Rotor Speed Waveform from Simulated Eccentric 3-Phase Induction Motor

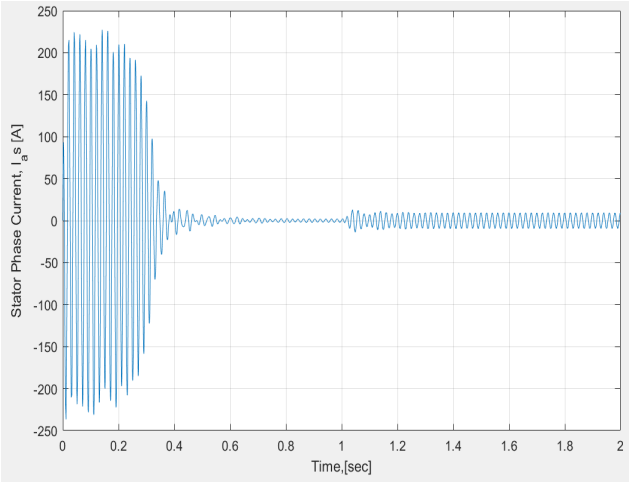

Fig 7 Stator Phase-Current Waveform from Simulated Healthy 3-Phase Induction Motor

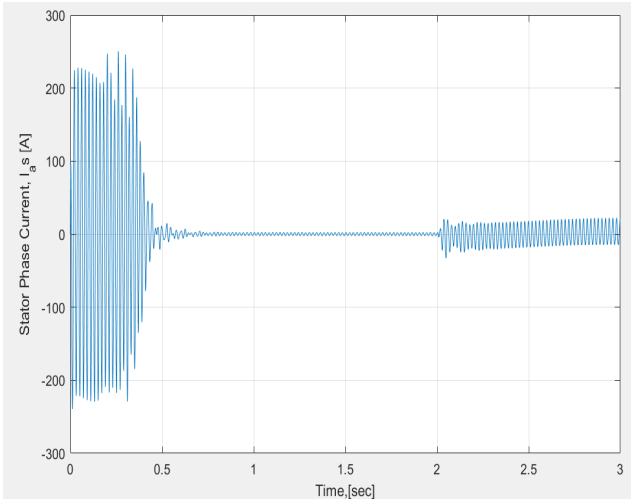

Fig 8 Stator Phase-Current Waveform from Simulated Eccentric 3-Phase Induction Motor

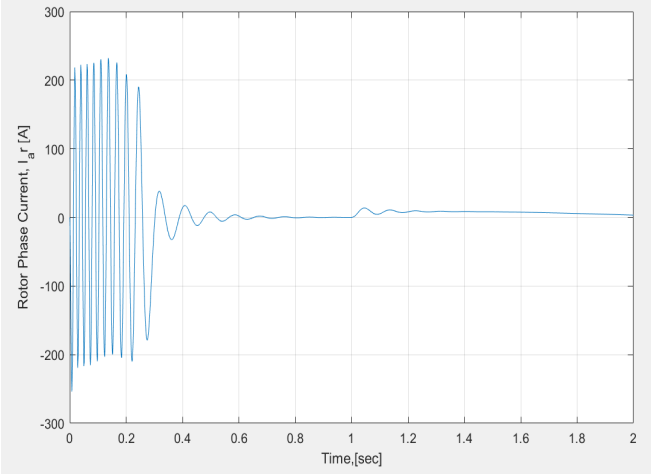

Fig 9 Rotor-Current Waveform from Simulated Healthy 3-Phase Induction Motor

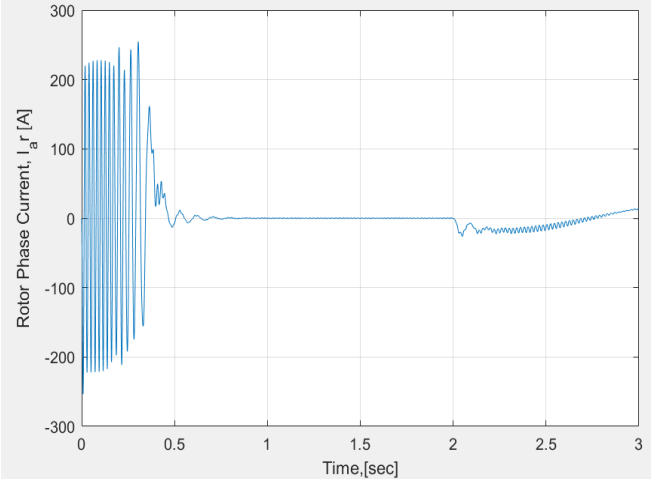

Fig 10 Rotor-Current Waveform from Simulated Eccentric 3-Phase Induction Motor

Journal of Newviews in Engineering and Technology (JNET)
Vol 2, Issue 1, March, 2020
Available online at http://www.rsujnet.org/index.php/publications/2020-edition

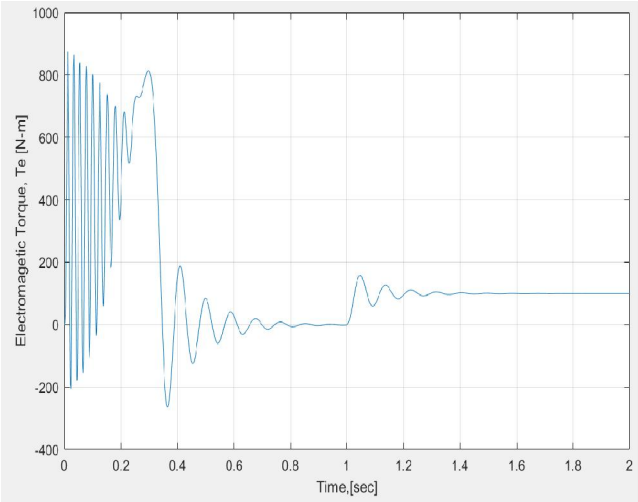

Fig 11 Electromagnetic Torque Waveform from Simulated Healthy 3-Phase Induction Motor

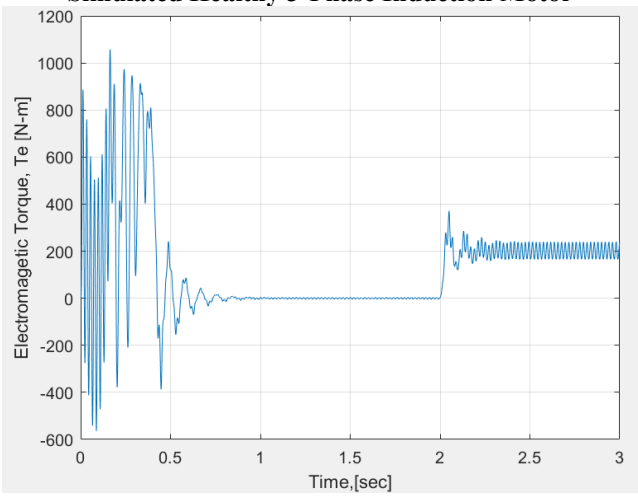

Fig 12 Electromagnetic Torque Waveform from Simulated Eccentric 3-Phase Induction Motor

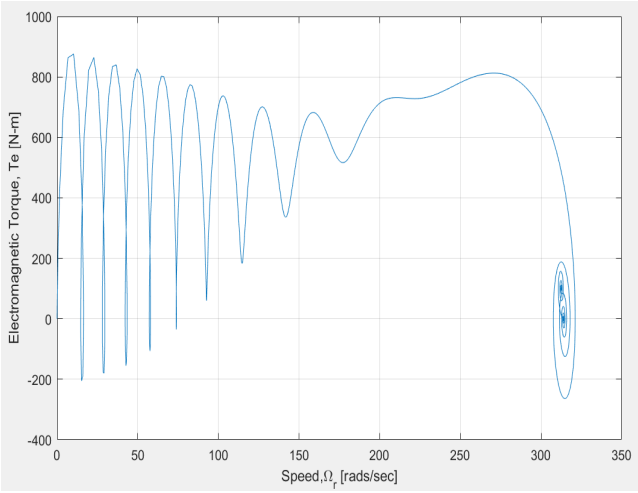

Fig 13 Electromagnetic Torque to Speed Waveform from Simulated Healthy 3-Phase Induction Motor

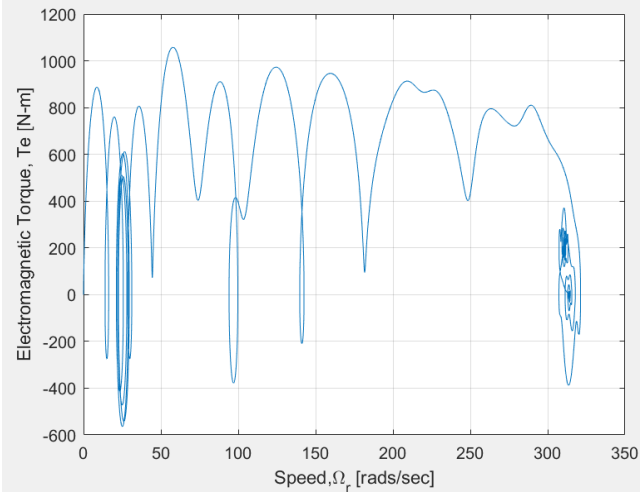

Fig 14 Electromagnetic Torque to Speed Waveform from Simulated Eccentric 3-Phase Induction Motor

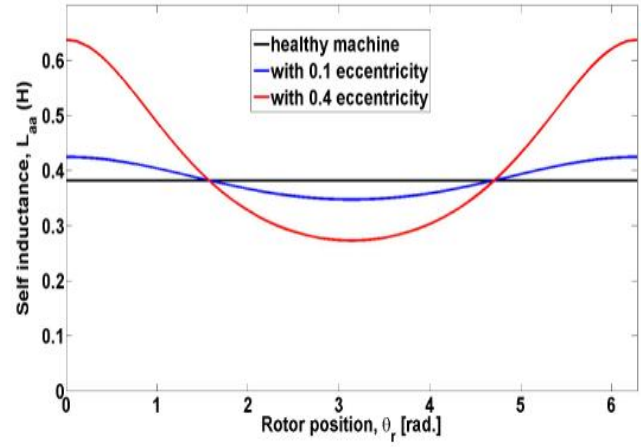

Fig 15 Plot of Self-Inductance of the Normal and Eccentric Machine with Eccentricities of ρ = 0.1 and 0.4

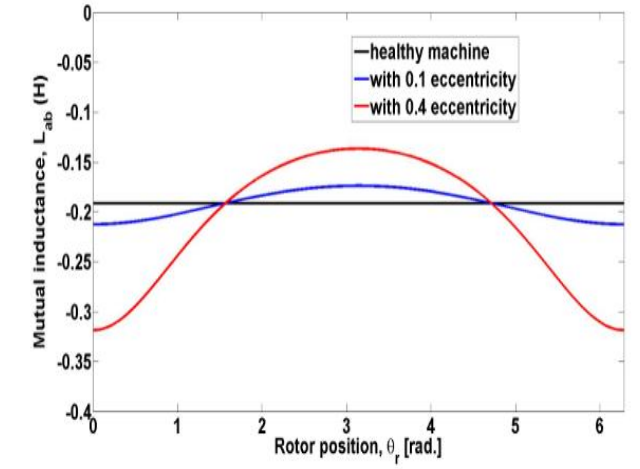

Fig 16 Plot of Mutual-Inductance of the Healthy and Eccentric Machine with Eccentricities of ρ = 0.1 and 0.4

Journal of Newviews in Engineering and Technology (JNET)
Vol 2, Issue 1, March, 2020
Available online at http://www.rsujnet.org/index.php/publications/2020-edition

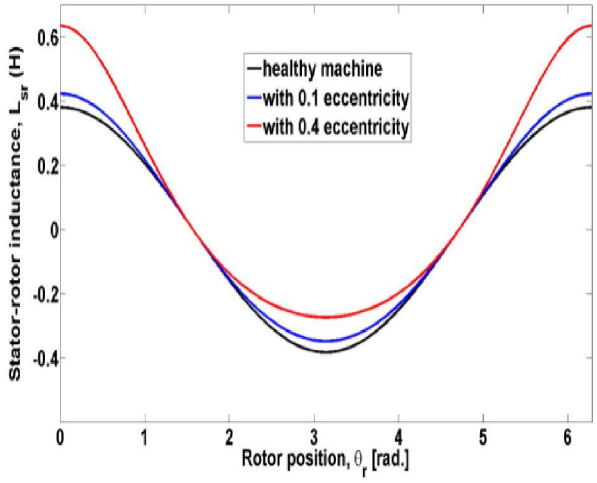

Fig 17 Plot of Stator-Rotor Inductance of the Healthy and Eccentric Machine with Eccentricities of ρ = 0.1 and 0.4

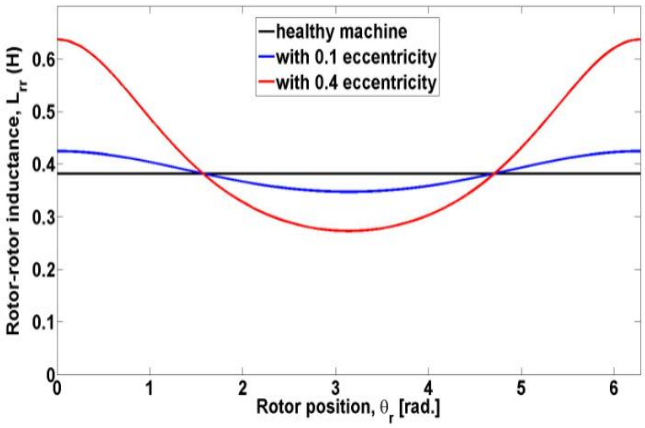

Fig 18 Plot of Stator-Rotor Inductance of the Healthy and Eccentric Machine with Eccentricities of ρ = 0.1 and 0.4

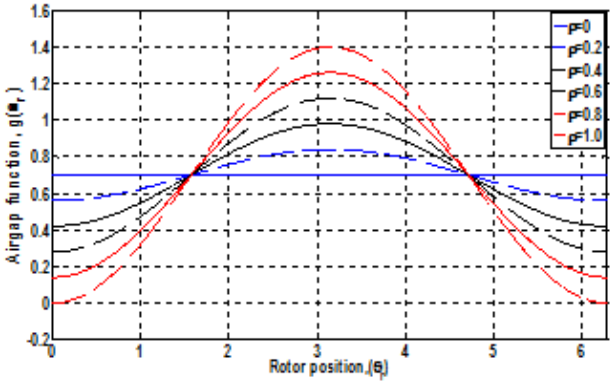

Fig 19 Plot of Air gap Function Showing Different Degrees of Eccentricity

From Fig. 19, it is easy to see that for ρ>0.7, g_0 goes higher than 1.0 at some points and hits zero at lowest values thereby validating the literatures cited earlier. Owing to the departure of the rotor from its nominal position as has been established, it is evident that the machine inductances must be recalculated with the new air gap function.

4. CONCLUSION:

In this paper, computer simulations for both healthy or concentric and eccentric induction motors were implemented using the matrices of integral calculus of the modeled circuitry voltage equation for a three-phase induction motor which is a differential function to generate the various characteristic waveforms of the motor quantities. These quantities are the speed, the current and the electromagnetic torque. The sum of effective inductances to develop an electromagnetic torque were modeled analytically. This work provides a proven MATLAB code that can be used by manufacturers of induction motors to assist in designing improved three-phase induction motors with little or no susceptibility for eccentricity

REFERENCES

Aderiano, M. (2006). Induction Motor Fault Diagnostic and Monitoring Methods. M. Eng. Dissertation, Marquette University, Milwaukee, Wisconsin, USA.

Ahmadi, M., Poshtan, J. & Poshtan, M. (2013). Static Eccentricity Fault Detection in Induction Motors using Wavelet Packet Decomposition and Gyration Radius. *Proceedings of 1st International Conference on Communications Signal Processing, and their Applications (ICCSPA)*, 12-14 February 2013, Sharjah, United Arab Emirates.

Almeida, A. T., Ferreira, F. J. T. E. & Baoming, G. (2014). Beyond Induction Motors—Technology Trends to Move Up Efficiency, *IEEE Transactions on Industry Applications*, 50 (3), 2103-2114.

Arkkio, A., Nepal, B. R. & Sinervo, A. (2017). Electromechanical Interaction in a Synchronous Reluctance Machine. International Symposium on Power Electronics Electrical Drives Automation and Motion (SPEEDAM), 14-16 June 2010, Pisa, Italy.

Bakhri, S. (2013). Detailed Investigation of Negative Sequence Current Compensation Technique for Stator Shorted Turn Fault Detection of Induction Motors. PhD Thesis, University of Adelaide, Australia.

Bouchikhi, E. H. E., Choqueuse, V. & Benbouzid M. E. H. (2013). Current Frequency Spectral Subtraction and its Contribution to Induction Machines Bearings Condition Monitoring. *IEEE Transactions on Energy Conversion*, 28(1), 135-144.

Chuan, H. & Shek, J. K. H. (2018). Calculation of Unbalanced Magnetic Pull in Induction Machines through Empirical Method. *IET Electric Power Applications,* 12 (9), 1233 - 1239

Dorrell, D. G. (1993). Calculation of Unbalanced Magnetic Pull in Cage Induction Machines. PhD Thesis, University of Cambridge, U.K.

Faiz, J., Ebrahimi, B. M., Akin, B. & Toliyat, H. A. (2010). Dynamic Analysis of Mixed Eccentricity Signatures at Various Operating Points and Scrutiny of Related Indices for Induction Motors. *IET Electric Power Applications*, 4 (1), 1-16.

Faiz, J. & Ojaghi, M. (2009). Unified Winding Function Approach for Dynamic Simulation of Different Kinds of Eccentricity Faults in Cage Induction Machines. *IET Electric Power Applications*, 3 (5), 461 – 470.

Ferreira, F. J. T. E. & Almeida, A. T. (2006). Method for In-field Evaluation of The Stator Winding Connection of Three-Phase Induction Motors to Maximize Efficiency and Power Factor. I*EEE Transactions on Energy Conversion*, 21 (2), 370-379.

Joksimovic, G. M. (2017). Dynamic Simulation of Cage Induction Machine with Airgap Eccentricity. *IEEE Electric Power Applications*, 152 (4), 703-731.

Joksimovic, G. M., Durovic, M. D., Penman, J. &. Arthur, N. (2000). Dynamic Simulation of Dynamic Eccentricity in Induction Machines- Winding Function Approach. *IEEE Transactions on Energy Conversion*, 15 (2), 143–148.

Nandi, S., Toliyat, H. A. & Li, X. (2005). Condition Monitoring and Fault Diagnosis of Electrical Motors - A Review. *IEEE Transactions on Energy Conversion*, 20, 719-729.

Obe, E.S. (2010). Calculation of Inductances and Variable Model of a Synchronous Reluctance Motor including all Slot and Winding Harmonics. *Energy Conversion and Management*, 52, 284–291.

Polat, A., Ertuğrul, Y.D. & Ergene, L.T. (2017). Static, Dynamic and Mixed Eccentricity of Induction Motor, IEEE 10th International Symposium on Diagnostics for Electrical Machines, Power Electronics and Drives (SDEMPED), 284-288.

Sen, P. C. (1999). Principles of Electric Machines and Power Electronics, Wiley.

Schimtz, N. L & Novotny, D.W. (1950). Introductory Electromechanics, The Ronald Press Company, New York.

Silwal, B., Rasilo, P., Perkkiö, L., Hannukainen, A., Eirola T. & Arkkio, A. (2016) Numerical Analysis of The Power Balance of An Electrical Machine with Rotor Eccentricity, IEEE Transactions on Magnetics, 52(3), 1-4.

Stephan, J. C. (2005). Electric Machinery Function Fundamentals, 4th Edition McGraw-Hill, New York.

Wasynczuk, O., Krause, P.C., Krause, P.C., Sudhoff S. D. & Pekarek, S. (2013). Induction Motor Drives, Analysis of Electric Machinery and Drive Systems, Hoboken, NJ: Wiley-IEEE Press.